Linear Viscoelastic Properties and Crystallization Behavior of Multi-Walled Carbon Nanotube/ Polypropylene Composites

Defeng Wu,[1,2] Yurong Sun,[1,2] Liang Wu,[1] Ming Zhang[1,2]

[1]*Department of Applied Chemistry, School of Chemistry and Chemical Engineering, Yangzhou University, Jiangsu 225002, People's Republic of China*
[2]*Provincial Key Laboratory of Environmental Material and Engineering, Jiangsu 225002, People's Republic of China*

Received 27 September 2007; accepted 29 November 2007
DOI 10.1002/app.27793
Published online 25 January 2008 in Wiley InterScience (www.interscience.wiley.com).

ABSTRACT: Multi-walled carbon nanotube/polypropylene composites (PPCNs) were prepared by melt compounding. The linear viscoelastic properties, nonisothermal crystallization behavior, and kinetics of PPCNs were, respectively, investigated by the parallel plate rheometer, differential scanning calorimeter (DSC), X-ray diffractometer (XRD), and polarized optical microscope (POM). PPCNs show the typical nonterminal viscoelastic response because of the percolation of nanotubes. The rheological percolation threshold of about 2 wt % is determined using Cole-Cole method. Small addition of nanotube can highly promote crystallization of PP matrix because of the heterogeneous nucleating effect. With increasing nanotube loadings, however, the crystallization rate decreases gradually because the mobility of PP chain is restrained by the presence of nanotube, especially at high loading levels. © 2008 Wiley Periodicals, Inc. J Appl Polym Sci 108: 1506–1513, 2008

Key words: polypropylene; multi-walled carbon nanotube; composites; rheology; crystallization

INTRODUCTION

In the field of composite materials, nano-reinforcing particles have stimulated much interest recently. Their main advantage over traditional reinforcements comes from their high aspect ratio and associated high surface-area-to-volume ratio. Owing to extraordinarily high elastic modulus, strength, and resilience,[1–3] carbon nanotubes (CNTs) including both single-walled (SWCNT) and multi-walled (MWCNT) ones promise to become the next-generation reinforcements for carbon nano-structured materials. Of particular interest is recently developed nanotube-based composites technology consisting of a polymer and CNTs. Three methods are commonly used to incorporate nanotubes into polymers: film casting of suspensions of nanotubes in dissolved polymers and polymerization of nanotubes-polymer monomer mixtures as well as melt mixing of nanotubes with polymers. Hitherto many polymer/nanotube composites have been prepared successfully via those approaches.[4] As expected from the high aspect ratio and high elastic modulus, experimentally introducing CNTs into a polymer matrix improves the mechanical properties and electrical conductivity of the original polymer matrix.

Among the most versatile polymer matrices are polyolefins, such as polypropylene (PP), which are very widely used because of their good balance between properties and cost, as well as their nice processability and low density. However, the mechanical and thermal properties are not sufficient for applications as engineering plastics. Therefore, PP is generally modified by melt mixing with nano-scaled clay[5–9] and fibers.[10,11] Recently, CNTs were also used as special nanofiller to prepare PP/CNTs composites, which provides a new way to obtain high performance PP engineering plastics. Many physical properties, such as crystallization behavior,[12–16] mechanical properties,[17–20] morphology,[21,22] thermal behavior,[20,22,23] and conductivity[24] of PP/CNTs composites were hence studied extensively.

It is well known that rheology is a powerful tool to examine mesco-structure of the filled polymer systems because the viscoelastic properties of those composite systems are highly related to the dispersion state of filler and the interactions between filler and polymer matrix. More important, both the processing and application of those nanocomposites requires information on their rheological responses. Therefore, in this work, at first we incorporated functionalized MWCNT into PP matrix via melt mix-

This article contains supplementary material available via the Internet at http://www.interscience.wiley.com/jpages/0021-8995/suppmat.

Correspondence to: D. Wu (dfwu@yzu.edu.cn).

Contract grant sponsor: Natural Science Foundation of Jiangsu Provincial Startup Program of Innovative Talent; contract grant number: BK2007559.

ing to obtain PP/MWCNT nanocomposites. Then, we conducted the linear rheological studies on those composites. The nonisothermal crystallization kinetics of composites was also studied, aiming at relating those behaviors to the mesoscopic structure of CNTs in the composites.

EXPERIMENTAL

Material preparation

Polypropylene (PP) (trade marked as 045, Yangzhou Petroleum Chemical Plant, China) used in this study is a commercially available isotactic homopolymer with a melt flow index of 4.0 g/10 min (230°C, 2.16 kg). MWNCT was supplied by Chengdu Organic Chemistry, Chinese Academy of Sciences. MQ1233 (purity > 95%), a carboxylic MWCNT, which is functionalized on purified MWCNT, is a chemical vapor deposition material with outside diameter of 10–20 nm, inside diameter of 5–10 nm, and length of 10–30 μm. The rate of surface carbon atom on MS1233 is about 8–10 mol % and the —COOH weight percent is about 1–6 wt % (measured by XPS).

PP/MWCNT composites (PPCNs, where *s* is the weight ratio of MWCNT) were prepared by direct melt compounding carboxylic MWCNT with PP in a HAAKE Polylab Rheometer (Thermo Electron, USA) at 180°C and 50 rpm for 8 min. The MWCNT loadings are 1, 2, 3, 5, and 7 wt %, respectively. For better comparison, the pure PP sample was also processed in Rheometer to keep identical thermal history with that of PPCNs. The sheet samples of about 1 mm thickness used for the following measurement were prepared by compression molding at 180°C and 10 MPa.

Microstructure characterization

The dispersion of MWCNT was investigated using a Tecnai 12 transmission electron microscope (TEM, PHILIPS, Netherlands) with 120 kV accelerating voltage. The microtomed sections is about 80–100 nm in thickness. The crystallographic structure of the neat PP and PPCNs was determined by a D8 ADVANCE X-ray diffractometer (XRD, BRUKER AXS, Germany) with Cu target and a rotating anode generator operated at 40 kV and 200 mA. The scanning rate was 2°/min from 10° to 60°. The crystallization morphology was studied using a polarized optical microscope (POM, LEICA BX51) equipped with a hot stage (Linklam LTM350). The same temperature ramps were used as in DSC testing.

Nonisothermal crystallization process

Nonisothermal Crystallization behavior was carried out on a NETZSCH DSC-204F1 differential scanning calorimeter (DSC). The samples about 5 mg in weight for DSC were cut from the film. In the nonisothermal crystallization process, the samples were melted at 180°C for 10 min to eliminate the previous thermal history and then cooled at the constant cooling rates of 5, 10, 15, and 20°C/min. The exothermal curves of heat flow as function of temperature were recorded to analyze nonisothermal crystallization process of the PP and its composites. All experiments were carried out under nitrogen.

Rheological measurements

Rheological measurements were carried out on the rheometer (HAAKE RS600, Thermo Electron USA) equipped with a parallel plate geometry using 20 mm diameter plates. All measurements were performed with a 200 FRTN1 transducer with low resolution limit of 0.02 g/cm. The sheet samples in thickness of 1.0 mm were first melted at 180°C for 5 min in the parallel plate fixture to eliminate residual thermal history, and then dynamic strain sweep was carried out to determine the linear viscoelastic region. At the strain level of 1%, the small amplitude oscillatory shear (SAOS) was applied and the dynamic frequency sweep were carried out on those samples.

RESULTS AND DISCUSSION

Microstructure of PPCNs

Figure 1 shows the TEM images of the PPCNs with various MWCNT loadings. At low loading level (2 wt %), MWCNTs are randomly oriented and well dispersed in the PP matrix, as can be seen in Figure 1(a). With increase of MWCNT loadings, however, MWCNTs tend to bundle together because intrinsic van der Waals attraction among the individual nanotubes in combination with high aspect ratio and surface area of the nanotubes, leads to some agglomeration. Thus at high loading levels (5 wt %), less uniformly dispersed and more entangled bundles of MWCNTs were formed, as shown in Figure 1(b).

Linear viscoelastic properties of PPCNs

Figure 2 shows the dependence of storage modulus (G') and complex viscosity (η^*) on frequency for pure PP and PPCNs. At low frequencies, PP chains are fully relaxed and exhibit typical homopolymer-like terminal behavior with the scaling properties of $G' \propto \omega^2$. However, this terminal behavior almost disappears even with small addition of MWCNTs, and the low-frequency G' increases remarkably by about 2 orders. Similar phenomenon has also been observed on PP/Clay nanocomposites[6,7] and other polymer/CNTs systems.[25–28] This nonterminal low

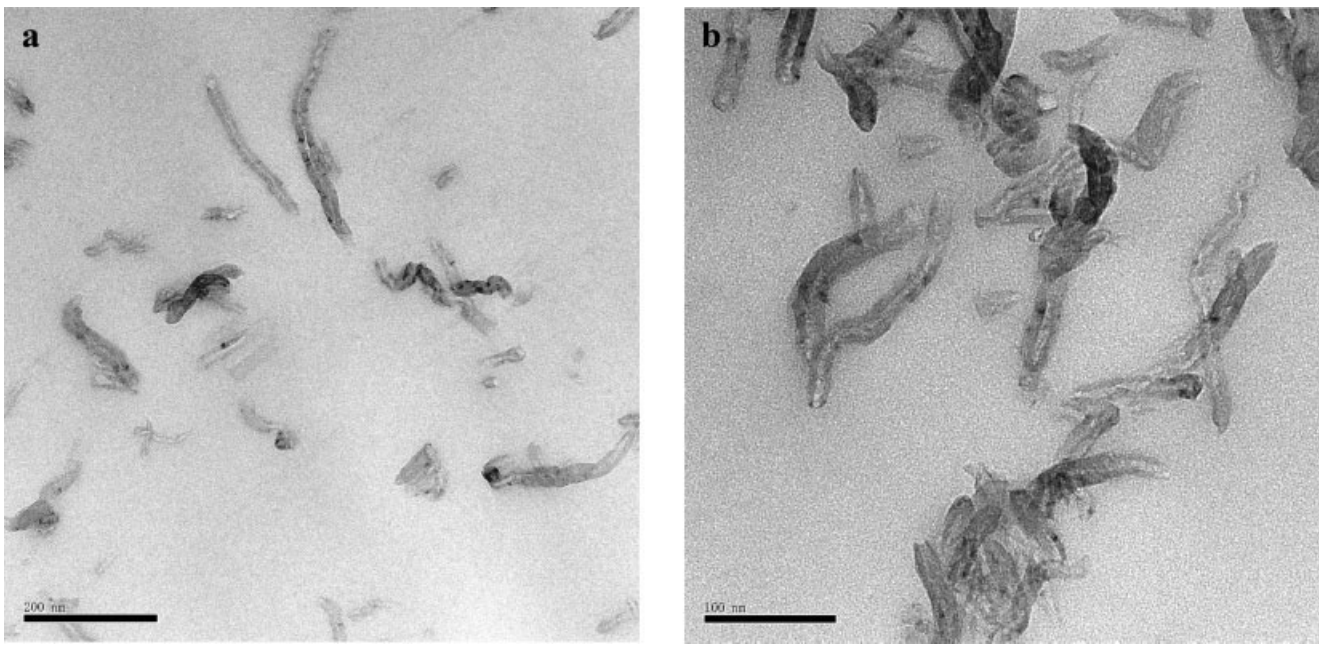

Figure 1 TEM image of (a) PPCN1 and (b) PPCN5 sample at the magnification of 97,000 and 195,000, respectively.

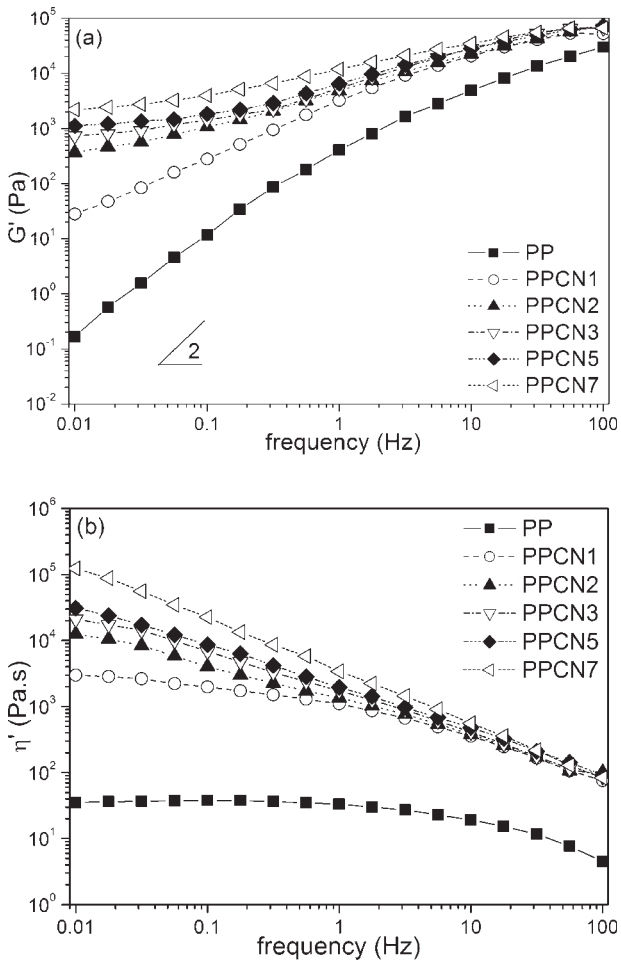

Figure 2 (a) Dynamic storage modulus (G') and (b) complex viscosity (η^*) for the PPCNs samples obtained in dynamic frequency sweep.

frequency behavior is attributed to the strong particle–particle interactions, which restrains the long-range motion of polymer chains. As a result, the low-frequency complex viscosity (η^*) increases with increasing MWCNT loadings and, the Newtonian plateau disappears gradually, showing a remarkable shear thinning behavior, as shown in Figure 2(b).

It is notable that the linear plateau of viscosity cannot be seen any more as the MWCNT loadings achieving up to 2 wt % and above, which is indicative of a transition from liquid to solid-like viscoelastic behavior. Cole-Cole plots[29] are often used for the description of viscoelastic properties (viscosity, modulus) of those materials with a relaxation time distribution such as heterogeneous polymeric systems because the relationship between imaginary viscosity (η'') versus real viscosity (η'') is very sensitive to the fluid–solid transition of a viscoelastic fluid. Figure 3 gives Cole-Cole plots for the PPCNs with various MWCNT loadings. Similar to neat PP, PPCN1 also presents single bulk relaxation arc, which indicates that small addition of MWCNTs has no remarkable influence on the relaxation behavior of PP chain in the experimental scale. However, further addition of MWCNTs changes the form of the Cole-Cole diagram from semicircular to linear one, which indicates that the presence of MWCNTs considerably retards the relaxation processes of PP matrix in the region of long relaxation times. In other words, the mesco-structure of nanotubes, percolation network, might form at present MWCNT loadings and, the long-range motion of polymer chains are restrained significantly as a result. Accordingly, the rheological percolation threshold for PPCNs is not

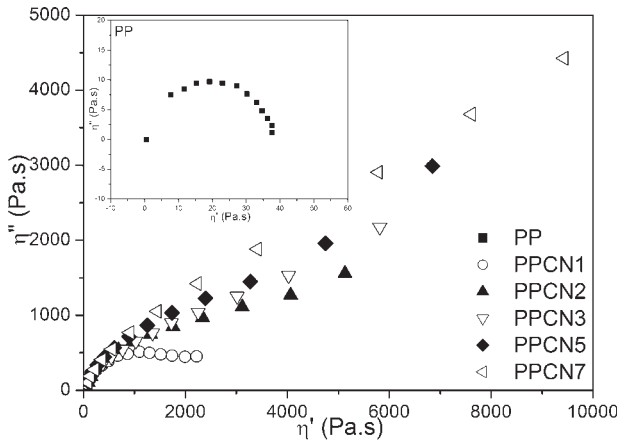

Figure 3 Cole-Cole plots of imaginary viscosity (η″) versus real viscosity (η′) for the neat PP and PPCNs samples.

more than 2 wt %, which is lower than that of corresponding clay-based nanocomposites. (PP/clay composites show the percolation threshold of 3–5 wt %[6,7]). This is due to larger radius of the hydrodynamic volume of CNTs because they present higher aspect ratio and flexibility compared with those of clay tactoids or platelets.

Crystalline morphology of PPCNs

It is well accepted that the mechanical and physical properties of the crystalline polymers are governed by the supermolecular morphology, which in turn is controlled by the crystallization process. POM observation was hence carried out to explore crystalline morphology of the neat PP and PPCNs after nonisothermal crystallization, as can be seen in Figure 4(a,b). For the neat PP, the micrograph exhibits a typical Maltese-cross spherulite. However, the nanocomposite presents far smaller spherulite size, which indicates that the presence of MWCNTs may act as nuclei to induce crystallization.

Figure 5 gives XRD patterns of the neat PP and its nanocomposites. It can be observed that there is a characteristic 2θ peak at 15.8° in the neat PP, corresponding to the hexagonal structure of β phase of PP matrix. [11,12,30] On the other hand no sign of this peak can be detected in the PPCNs, except for the characteristic peaks of monoclinic α phase[31,32] at 14.0° (110), 17.0° (040), 18.6° (130), and 21.0° (111,131). In addition, no difference in crystal phase among PPCNs themselves can be seen. It indicates that the partial phase transform from α to β structure is hard to occur on the PP matrix during crystallization process in the presence of MWCNTs. This is contrary to those observed on the clay-based[8,9] and SWCNT-based PP nanocomposites.[12] In other words, unlike that of clay platelets or SWCNT, MWCNT can only promote formation of α crystal phase of PP matrix. Similar phenomenon has also been observed by Assouline et al.[13]

Scherrer equation is generally used to estimate the crystallite size basing on the diffraction pattern.[33] The crystallite dimension, L_{hkl} can be calculated by:

$$L_{hkl} = \frac{K\lambda}{\beta_{hkl} \cos \theta_{hkl}} \quad (1)$$

where L_{hkl} is the crystallite dimension or coherence length perpendicular to the (hkl) plane, K is the Scherrer constant, λ is the wavelength of the X-rays, and θ is the Bragg angle. When β_{hld} is the diffraction half-width, K takes a value of 0.9. The results are listed in Table I. Clearly, the crystallite size perpendicular to the α crystal plane like (040), (130), (111), and (041) in PPCNs is smaller than that of neat PP, which confirms that MWCNT acts as heterogeneous nucleating agent during crystallization of PP matrix.

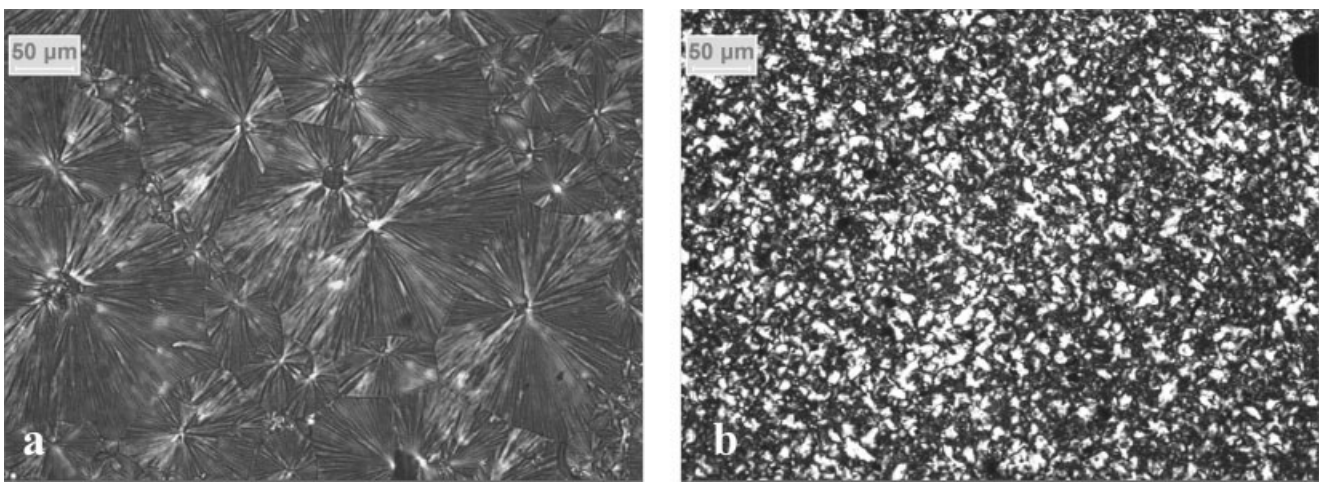

Figure 4 POM images of (a) neat PP and (b) PPCN1 samples.

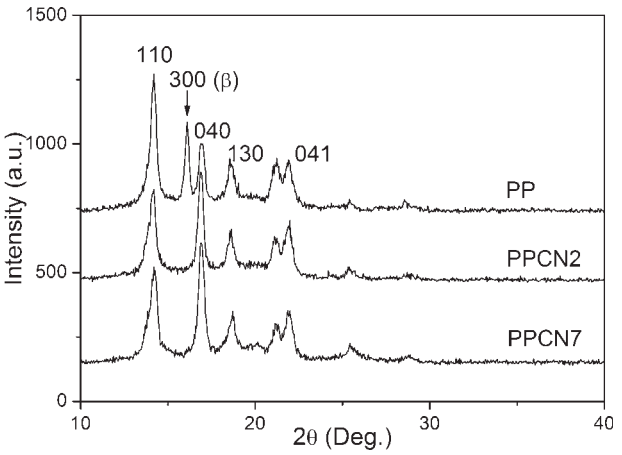

Figure 5 XRD patterns of the neat PP and PPCNs samples.

Nonisothermal crystallization kinetics

Figure 6(a,b) shows the nonisothermal crystallization and melt curves at identical cooling rate for neat PP and its nanocomposites. The calorimetric parameters are listed in Table II. T_c and T_m are the temperature of crystallization and melting peak, respectively. ΔH_c and ΔH_m are the corresponding enthalpies normalized to unit mass. Compared with that of neat PP, T_c of PPCNs shows a remarkable increase by about 10°C even at very low loading levels of MWCNT (1 wt %). It confirms again that MWCNT acts as the additional active substrates, promoting crystallization of PP matrix. This heterogeneous nucleation, however, also leads to the formation of more defect ridden crystalline lamella and less ordered crystals of PP, decreasing ΔH_c as a result. In other words, the presence of MWCNT reduces the ability of polymers chains to be fully incorporated into growing crystalline lamella. Thus, the T_m of PPCNs decreases gradually with increasing MWCNT loadings, as can be seen in Figure 6(b). In addition, the multi-melting behavior of neat PP [see the arrow in Fig. 6(b)], which is attributed to the visible difference of T_m between β and α crystal form,[30,31] cannot be seen on the PPCNs. It further confirms that MWCNT only plays as α nucleating agent on the crystallization of PP matrix.

TABLE I
Crystallite Dimension of Neat PP and PPCNs Samples

Samples	L_{110}(nm)	L_{040}(nm)	L_{130}(nm)	L_{111}(nm)	L_{041}(nm)
PP	9.7	11.5	10.8	12.5	10.2
PPCN1	10.0	9.3	10.3	11.3	8.6
PPCN2	10.2	9.8	10.5	11.3	8.8
PPCN3	10.2	9.8	9.8	11.0	8.8
PPCN5	10.5	8.7	10.1	10.2	9.0
PPCN7	10.3	8.8	9.5	10.5	8.6

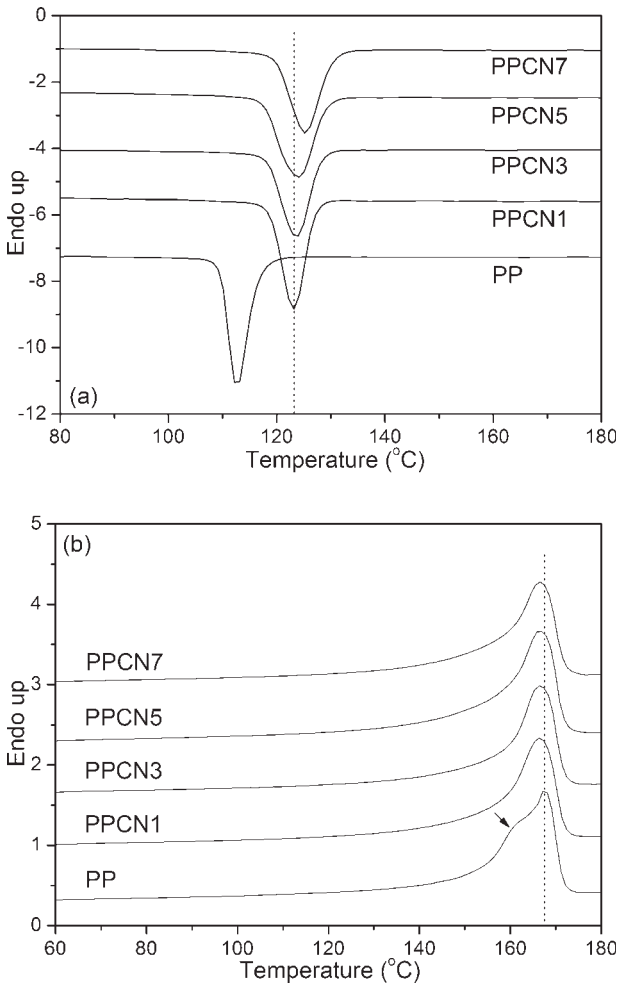

Figure 6 The DSC thermogram of neat PP and PPCNs samples for (a) crystallization and (b) melting process.

To explore more clearly how the MWCNT and its mescoscopic structure influence the crystallization process of PP matrix, it is necessary to study the crystallization kinetics of PPCNs. The relative degree of crystallinity (X_t), as a function of crystallization temperature (T), is defined as

$$X_t = \int_{T_o}^{T} (dH_c/dT)dT \Big/ \int_{T_o}^{T_\infty} (dH_c/dT)dT \qquad (2)$$

where T_o and T_∞ represent the onset and the end of crystallization temperature, respectively. Although MWCNT promotes the α form, but there is only a slight difference in melting enthalpy between α and β form (which are 178 and 170 J/g, respectively[30]). This cannot cause a significant impact on the kinetics model for PP. Figure 7(a) shows the typical relative crystallinity curves for the neat PP and PPCNs. The results of half crystallization time $t_{1/2}$ are listed in Table II. The relative crystallization rate (at identical cooling rate) can be determined from the slope in the crystallization region, as indicated by the line

TABLE II
Calorimetric Data and Kinetics Parameter for neat PP and PPCNs Samples

Samples	T_c (°C)[a]	ΔH_c (J/g)[a]	T_m (°C)[a]	ΔH_m (J/g)[a]	$t_{1/2}$ (min)[a]	n[a]	α[b]	$F(T)$[b]	ΔE (kJ/mol)
PP	112.7	106.8	166.6	105.8	1.2	4.3	1.36	18.3	216.3
PPCN1	122.2	106.6	166.2	105.3	0.62	3.4	1.35	13.6	245.2
PPCN2	122.6	105.9	165.8	103.3	0.65	3.2	1.38	14.8	250.6
PPCN3	123.8	104.1	165.3	102.2	0.72	3.2	1.32	14.5	253.4
PPCN5	124.0	101.1	165.3	102.2	0.81	3.0	1.33	15.3	258.5
PPCN7	125.3	101.3	165.4	99.1	0.95	2.8	1.28	16.2	268.7

[a] Obtained from the cooling scan at the rate of 10°C/min.
[b] Thr relative crystallinity (X_t%) is presumed as 40%.

arrow in Figure 7(a). It is clear that PPCNs show higher crystallization rate than that of neat PP. However, with increase of MWCNT loadings, the crystallization rate decreases gradually, resulting in a monotonous increase of $t_{1/2}$ for PPCNs samples. As mentioned in the rheology section, the motion of PP chain segments in the PPCNs is highly restrained by the presence of MWCNTs, especially at high loading levels, leading to a sharp increase of viscosity. Thus, it is reasonable to propose that MWCNT presents two disparate effects on the crystallization of PP matrix: the nucleation effect promotes the crystallization, while the impeding effect decreases crystallization rate especially at high loading level of MWCNT or in the case of percolation.

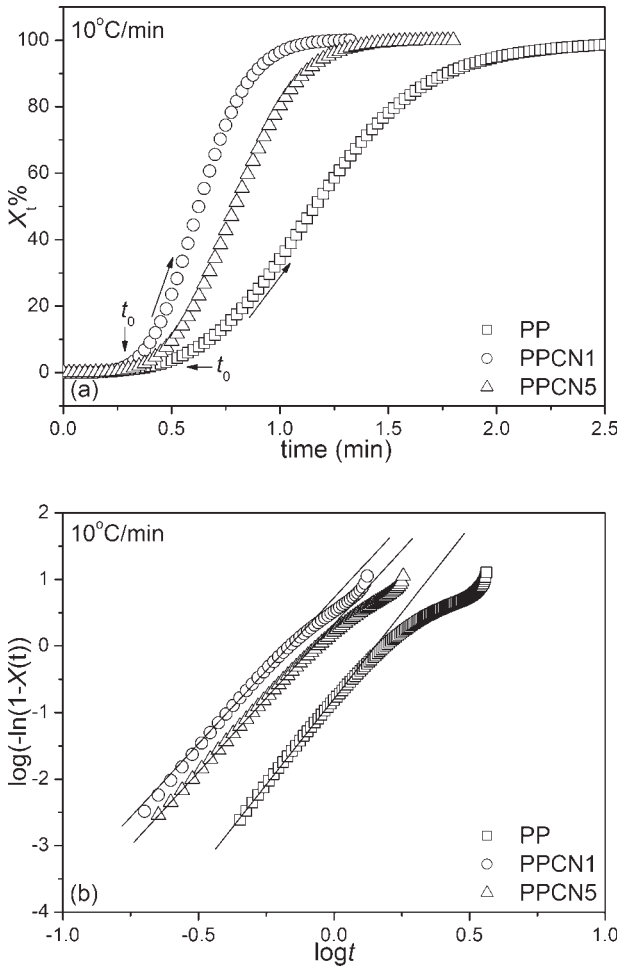

Figure 7 (a) The curves of relative crystallinity versus temperatures and (b) corresponding Avrami plots for the neat PP and PPCNs samples at the cooling rate of 10°C/min.

In general, the Avrami equation[34] can also be used to describe nonisothermal crystallization:

$$X(t) = 1 - \exp(-kt^n) \tag{3}$$

$$\log[-\ln(1 - X(t))] = n \log t + \log k \tag{4}$$

where $X(t)$ is relative crystallinity at crystallization time, t, n is the Avrami exponent, k is the crystallization rate constant. The plots of $\log[-\ln(1 - X(T))]$ versus $\log t$ are shown in Figure 8 and the Avrami exponent n obtained are listed in Table II. But in this case, the Avrami parameters lost their physical meanings and can only be used for qualitative comparison because temperature changes constantly during nonisothermal crystallization.

Mo and coworkers[35] developed an approach to study nonisothermal crystallization kinetics of polymers systems. For the nonisothermal crystallization process, physical variables relating to the process are relative degree of crystallinity, X_t, heating rate, ϕ, and crystallization temperature, T. By rearranging Avrami equations at a given relative crystallinity X_t:

$$\ln \phi = \ln F(T) - \alpha \ln t \tag{5}$$

where $F(T) = [K(T)/Z_t]^{1/m}$ refers to the value of heating rate, which must be chosen within unit crystallization time when the measured system amounts to a certain degree of crystallinity. The parameter $K(T)$ is cooling or heating function, m is the Ozawa exponent that depends on the dimension of the crystal growth, and z_t is a composite rate constant involving both nucleation and growth rate parameters. According to eq. (5), at a given degree of crystallinity, plots of $\ln \phi$ versus $\ln t$ yields good linear

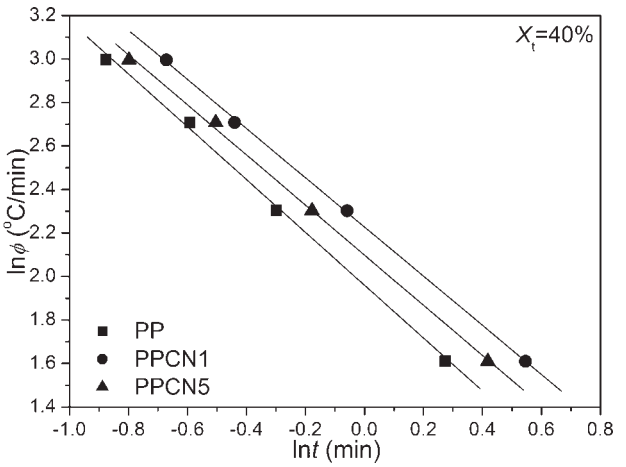

Figure 8 Mo plots of ln ϕ versus ln t for the neat PP and PPCNs samples at a given relative crystallinity of 40%.

relationship between ln ϕ and ln t, which suggests that Mo model can provide a satisfactory description on the nonisothermal crystallization for PPCNs samples, as can be seen in Figure 8. The kinetic parameters, $F(T)$ and α, which are determined from the intercept and slope of those lines, are listed in Table II.

It can be seen that at a certain relative degree of crystallinity, the value of $F(T)$ for the PPCNs is smaller than that for neat PP, that is, the nanocomposites require lower heating rate to approach the identical relative degree of crystallinity. In other words, the crystallization rate of PPCNs is higher than neat PP. It is notable that the value of $F(T)$ increases with increasing MWCNT loadings, again indicating that MWCNT and its percolation network structure may have impeding effect on the crystallization of PP matrix. Hence the Kissinger model[36] was used to determine the activation energy, ΔE, for the transport of the macromolecular segments to the growing surface.

$$\frac{d[\ln(\phi/T_p^2)]}{d(1/T_p)} = \frac{-\Delta E}{R} \tag{6}$$

where R is the gas constant and ϕ is the cooling rate. The values of ΔE are also listed in Table II. As expected, on adding small amounts of MWCNTs (1 wt %) to the pure PP, the values of ΔE increase significantly, because the MWCNT increases the viscosity of the composite system, hindering rearrangement of the PP macromolecule segments and increasing the ΔE value as a result. Therefore, nanotube acts as a heterogeneous nucleating agent to facilitate crystallization and also as a physical hindrance to retard crystallization. Of these, which one acts as a dominant role mainly lies on the loading levels and the thermodynamic conditions.

CONCLUSIONS

In this study, PPCNs were prepared by melt mixing for rheological and crystallization measurements. The results show that PPCNs presents solid-like rheological response under SAOS flow as the MWCNT loadings achieving up to 2 wt %, which is attributed to the percolation of nanotubes. The presence of MWCNT promotes crystallization of PP matrix because of the heterogeneous nucleating effect. But the MWCNT also retards rearrangement of the PP chain segments to some extent, reducing crystallization kinetics at high loading levels.

References

1. Iijima, S. Nature 1991, 354, 56.
2. Subramoney, S. Adv Mater 1998, 10, 1157.
3. Salvetat, J. P.; Briggs, G. A. D.; Bonard, J. M.; Bacsa, R. R.; Kulik, A. J.; Stockli, T.; Burnham, N. A.; Forro, L. Phys Rev Lett 1999, 82, 944.
4. Moniruzzaman, M.; Winey, K. I. Macromolecules 2006, 39, 5194.
5. Kawasumi, M.; Hasegawa, N.; Kato, M.; Usuki, A.; Okada, A. Macromolecules 1997, 30, 6333.
6. Solomon, M. J.; Almusallam, A. S.; Seefeldt, K. F.; Somwangthanaroj, A.; Varadan, P. Macromolecules 2001, 34, 1864.
7. Li, J.; Zhou, C. X.; Wang, G.; Zhao, D. L. J Appl Polym Sci 2003, 89, 3609.
8. Zhao, L. J.; Li, J.; Guo, S. Y.; Du, Q. Polymer 2006, 47, 2460.
9. Li, J.; Ton-That, M. T.; Leelapornpisit, W.; Utracki, L. A. Polym Eng Sci 2007, 47, 1447.
10. Wu, C. M.; Chen, M.; Karger-Kocsis, J. Polym Bull 1998, 41, 239.
11. Assouline, E.; Pohl, S.; Fulchiron, R.; Gerard, J.-F.; Lustiger, A.; Wagner, H. D.; Marom, G. Polymer 2000, 21, 7843.
12. Grady, B. P.; Pompeo, F.; Shambaugh, R. L.; Resasco, D. E. J Phys Chem B 2002, 106, 5852.
13. Assouline, E.; Lustiger, A.; Barber, A. H.; Cooper, C. A.; Klein, E.; Wachtel, E.; Wagner, H. D. J Polym Sci Part B: Polym Phys 2003, 41, 520.
14. Leelapornpisit, W.; Ton-That, M. T.; Perrin-Sarazin, F.; Cole, K. C.; Denault, J.; Simard, B. J Polym Sci Part B: Polym Phys 2005, 43, 2445.
15. Zhou, Z.; Wang, S. F.; Lu, L.; Zhang, Y.; Zhang, Y. X. J Polym Sci Part B: Polym Phys 2007, 45, 1616.
16. Wang, K.; Tang, C. Y.; Zhao, P.; Yang, H.; Zhang, Q.; Du, R. N.; Fu, Q. Macromol Rapid Commun 2007, 28, 1257.
17. Zhang, H.; Zhang, Z. Eur Polym J 2007, 43, 3197.
18. Xiao, Y.; Zhang, X. Q.; Cao, W.; Wang, K.; Tan, H.; Zhang, Q.; Du, R. N.; Fu, Q. J Appl Polym Sci 2007, 104, 1880.
19. Zhao, P.; Wang, K.; Yang, H.; Zhang, Q.; Du, R. N.; Fu, Q. Polymer 2007, 48, 5688.
20. Ganb, M.; Satapathy, B. K.; Thunga, M.; Weidisch, R.; Potschke, P.; Janke, A. Macromol Rapid Commun 2007, 28, 1624.
21. Avila-Orta, C. A.; Medellin-Rodriguez, F. J.; Davila-Rodriguez, M. V.; Aguirre-Figueroa, Y. A.; Yoon, K.; Hsiao, B. S. J Appl Polym Sci 2007, 106, 2640.
22. Jose, M. V.; Dean, D.; Tyner, J.; Price, G.; Nyairo, E. J Appl Polym Sci 2007, 103, 3844.
23. Marosfi, B. B.; Szabo, A.; Marosi, G.; Tabuani, D.; Camino, G.; Pagliari, S. J Therm Anal Cal 2006, 86, 669.
24. Alig, I.; Lellinger, D.; Dudkin, S. M.; Potschke, P. Polymer 2007, 48, 1020.

25. Potschke, P.; Fornes, T. D.; Paul, D. R. Polymer 2002, 43, 3247.
26. Potschke, P.; Abdel-Goad, M.; Alig, I.; Dudkin, S.; Lellinger, D. Polymer 2004, 45, 8863.
27. Wu, D. F.; Wu, L.; Zhang, M. J Polym Sci Part B: Polym Phys 2007, 45, 2239.
28. Wu, D. F.; Wu, L.; Sun, Y. R.; Zhang, M. J Polym Sci Part B: Polym Phys 2007, 45, 3137.
29. Cole, K. S.; Cole, R. H. J Chem Phys 1941, 9, 341.
30. Li, J. X.; Cheung, W. L.; Jia D. M. Polymer 1999, 40, 1219.
31. Assouline, E.; Wachtel, E.; Grigull, S.; Lustiger, A.; Wagner, H. D.; Mamm, G. Polymer 2001, 42, 6231.
32. Fanegas, N.; Gomez, M. A.; Marco, C.; Jimenez, I.; Ellis, G. Polymer 2007, 48, 5324.
33. Kakudo, M.; Kasai, N. X-ray Diffraction by Polymers; Kodansha: Tokyo, 1972.
34. Avrami, M. J Chem Phys 1939, 7, 1103.
35. Liu, T. X.; Mo Z. S.; Wang, S.; Zhang, H. F. Polym Eng Sci 1997, 37, 568.
36. Kissinger, H. J Res Natl Stand 1956, 57, 217.